Advanced Robotics

ISSN: 0169-1864 (Print) 1568-5535 (Online) Journal homepage: http://www.tandfonline.com/loi/tadr20

Conformational Modeling of Continuum Structures in Robotics and Structural Biology: A Review

G.S. Chirikjian

To cite this article: G.S. Chirikjian (2015) Conformational Modeling of Continuum Structures in Robotics and Structural Biology: A Review, Advanced Robotics, 29:13, 817-829, DOI: 10.1080/01691864.2015.1052848

To link to this article: http://dx.doi.org/10.1080/01691864.2015.1052848

Advanced Robotics, 2015
Vol. 29, No. 13, 817–829, http://dx.doi.org/10.1080/01691864.2015.1052848

Taylor & Francis
Taylor & Francis Group

SURVEY PAPER

Conformational Modeling of Continuum Structures in Robotics and Structural Biology: A Review

G.S. Chirikjian*

Department of Mechanical Engineering, Johns Hopkins University, Baltimore, MD 21218, USA

(*Received 31 August 2014; revised 12 April 2015; accepted 30 April 2015*)

Hyper-redundant (or snakelike) manipulators have many more degrees of freedom than required to position and orient an object in space. They have been employed in a variety of applications ranging from search-and-rescue to minimally invasive surgical procedures, and recently they even have been proposed as solutions to problems in maintaining civil infrastructure and the repair of satellites. The kinematic and dynamic properties of snakelike robots are captured naturally using a continuum backbone curve equipped with a naturally evolving set of reference frames, stiffness properties, and mass density. When the snakelike robot has a continuum architecture, the backbone curve corresponds with the physical device itself. Interestingly, these same modeling ideas can be used to describe conformational shapes of DNA molecules and filamentous protein structures in solution and in cells. This paper reviews several classes of snakelike robots: (1) hyper-redundant manipulators guided by backbone curves; (2) flexible steerable needles; and (3) concentric tube continuum robots. It is then shown how the same mathematical modeling methods used in these robotics contexts can be used to model molecules such as DNA. All of these problems are treated in the context of a common mathematical framework based on the differential geometry of curves, continuum mechanics, and variational calculus. Both coordinate-dependent Euler–Lagrange formulations and coordinate-free Euler–Poincaré approaches are reviewed.

Keywords: hyper-redundant manipulators; variational calculus; Lie group; continuum model; biological macromolecule

1. Introduction

Snakelike, wormlike, tentacle, elephant-trunk, or 'hyper-redundant' manipulators and mobile robots have been studied extensively over the past few decades. Such manipulators can have either a discrete or continuum architecture. In either case, it is convenient to use continuous curves to describe their overall shape. Inspired by the exterior appearance and functionality of their biological counterparts, the design principles for these robotic devices vary from biologically inspired internal morphologies, on the one hand, to completely different architectures such as variable-geometry-trusses and continuum manipulators, on the other. Moreover, these devices can either be fully actuated or under-actuated, such as in medical applications in which small size and the ability to easily sterilize instruments are critical.

This paper is a review that covers the mathematical methods used to model the kinematics and mechanics of continuum filaments. Interestingly, many of these modeling methods also find applications in modeling the behavior of DNA and filamentous protein molecules. In this way, the study of hyper-redundant manipulator kinematics has had some connection to the field of molecular biophysics, thereby extending the reach of these methods beyond their original application domain. This section reviews the literature on snakelike robots and their application areas, and provides background mathematics for use in the remainder of the paper. Before proceeding to the technical discussion, some brief remarks about the history of snakelike robots are in order.

Hirose and collaborators initiated the study of snakelike robots in the early 1970s, as summarized in [1]. Over the years, snakelike locomotion systems [2] have been designed for search-and-rescue.[3] Elastic-filament manipulators have been used for positioning and orienting objects, as well as for nasal and throat surgeries.[4,5] Steerable needle concepts and associated nonholonomic planning have been proposed for minimally invasive biopsy and treatment procedures.[6–8] Continuum [9,10] and concentric elastic tube robots [11–13] have been proposed for a variety of tasks including medical procedures. And hyper-redundant manipulators have been proposed for satellite servicing and inspection in nuclear power plants.

Continuum manipulators have become popular in recent years,[14,15] including applications such as grasping. [16–18] Often, researchers in this field point to [19] as the

*Email: gregc@jhu.edu

starting point for the study of such manipulators. However, as clearly stated in [20], the use of continuous backbone curves can be used for either hyper-redundant manipulators with discrete or continuous (aka continuum) morphologies. Bio-inspired structures such as tentacles [21,22] and associated locomotion [23,24] continue to be basic research problems of interest. On the applied side, the mechanics [25] and sensing [26] within active endoscopes [27,28] have been receiving increasing attention in recent years.

The mechanics of continuum filaments is by no means new and has been reinvented many times over the past 250 years. In fact, Euler studied these objects in the eighteenth century, and they have come to be known as 'Euler's elastica.' In the nineteenth century, Kirchhoff and Clebsch studied these objects, and at the beginning of the twentieth century, F. and E. Cosserat introduced their nonlinear theory of rods. For the history of elastic curves and pointers to the mechanics literature see [29–31].

Also predating the study of continuum manipulators is the use of elastic curves forced by Brownian motion in the polymer physics literature. Such models have been used for DNA and other 'semi-flexible' or 'stiff' macromolecules for more than 50 years.[32–35] Experimental determination of the stiffness of DNA has been reported in [36–38] and theoretical and computational results have been put forth to model the elasticity of DNA and other filamentous biomolecular structures.[39–46] The efficacy of continuum elastic models of DNA in the case of long chains (e.g. a hundred base pairs or longer) have been documented, as have the limitations of such models for very short segments. [47,48]

Elastic models of DNA mechanics has a long history. [49,50] A number of studies on chiral and uncoupled end-constrained elastic rod models of DNA with circular cross-section have been presented.[51,52] More recent works involve the modeling of DNA as an anisotropic inextensible rod and also include the effect of electrostatic repulsion for describing the DNA loops bound to Lac repressor, etc. [53,54]. Another recent work includes sequence-dependent elastic properties of DNA.[55] All of these aforementioned works are based on Kirchhoff's thin elastic rod theory.[31] This theory, as originally formulated, deals with nonchiral elastic rods with circular cross-section. Simo and Vu-Quoc formulated a finite element method using rod theory.[30] Coleman et al. reviewed dynamical equations in the theories of Kirchhoff and Clebsch [56]. Gonzalez and Maddocks devised a method to extract sequence-dependent parameters for a rigid base pair DNA model from molecular dynamics simulation.[57] Another recent work includes the application of Kirchhoff rod theory to marine cable loop formation and DNA loop formation.[58]

This paper focuses on snake robots with a fixed base (such as the one shown in Figure 1 which consists of multiple platforms stacked to form a hybrid manipulator), and shows how these same models are applicable to filamentous biomolecular structures such as DNA. Therefore, locomotion systems are not modeled here, but it is worth mentioning that snakelike [59,60] and wormlike [24,61] locomotion based on the propagation of peristaltic waves and other modalities [62,63] have continued to receive significant attention in the literature.

The remainder of this paper is structures as follows. Section 2 reviews the concept of a 'backbone curve' that can be used to either approximate a discrete chain or exactly model the kinematics and dynamics of a continuum filament. Along with this concept, a simple method for inverse kinematics involving a superposition of modes is discussed. Section 3 reviews the variational methods that are applicable of generating the conformations and optimal framing of elastic curves as applied to manipulators, tubes, and DNA molecules. In particular, when using coordinates, the Euler–Lagrange equations provide necessary conditions for optimality, and in the coordinate-free setting, the Euler–Poincaré equations play the same role. Section 4 focuses on a special class of problems in which global optimality can be ensured. These include the optimal framing and reparameterization of space curves. Section 5 then discusses optimal backbone curve shapes generated using both parameterizations of rigid body motions, and how this same problem can be formulated without coordinates, and demonstrates the methodology on DNA loops. That section also discusses the variational modeling of concentric tube (active cannula) devices and illustrates how these same methods can be applied in needle steering.

2. Continuum modeling of slender structures

Similar questions arise in: (1) the redundancy resolution of fully actuated, hyper-redundant, manipulators; (2) the mechanical analysis and planning of under-actuated snakelike systems (flexible needles and active cannulae); and (3) DNA mechanics. In all of these cases, the physical structure can be described by a *backbone curve* of the form

$$\mathbf{x}(t) = \int_0^t [1 + \epsilon(\tau)] R(\tau) \mathbf{e}_1 \, \mathrm{d}\tau \tag{1}$$

for $t \in [0, 1]$, where $\mathbf{e}_1 = [1, 0, 0]^T$ and T denotes the transpose. $R(\tau)\mathbf{e}_1$ is the unit tangent vector, defined relative to a 3×3 rotation matrix, $R(\tau) \in SO(3)$ for any value $\tau \in [0, t]$, and $\epsilon(t) > -1$ is a function that describes how much the curve parameter deviates from arc length. (When $\epsilon(t) = 0$, the parameter t becomes arc length.)

Equation (1) can be thought of as the infinite limit of a cascade of infinitesimally small serial links, each enumerated by a value of τ, the orientation of each given by $R(\tau)\mathbf{e}_1$, and if a link itself is a prismatic joint, then the degree to which it can stretch or shrink is described by $\epsilon(\tau)$.

From basic Calculus, the tangent to this curve is

$$\frac{\mathrm{d}\mathbf{x}}{\mathrm{d}t} = [1+\epsilon(t)]R(t)\mathbf{e}_1.$$

This is a vector with magnitude $\|\mathrm{d}\mathbf{x}/\mathrm{d}t\| = 1+\epsilon(t)$. When $\epsilon(\tau) \equiv 0$, the tangent $\mathrm{d}\mathbf{x}/\mathrm{d}t$ becomes a unit vector and the curve parameter becomes arc length. Here t is a curve parameter which should not be confused with time (there is no time variable in the current context). Moreover, t is used here instead of s (arc length) to allow for greater generality.

2.1. The modal approach

A question that arises immediately is how to perform inverse kinematics for slender continuum structures described by a curve such as that in (1). A natural approach is to restrict the curve to a limited set of 'extrinsic modes.' For example, one can choose a spline-like curve of the form

$$\mathbf{x}(t) = \sum_{k=1}^{m} b_k \mathbf{\Phi}_k(t) \tag{2}$$

for some set of predefined shape functions $\{\mathbf{\Phi}_k\}$ and limit m to match the number of degrees of freedom needed to complete some task such as positioning the hand located at the point $t = 1$. For example, $m = 2$ to position in the plane, $m = 3$ to position and orient in the plane, $m = 3$ to position in space, and $m = 6$ to position and orient in space. Early in the study of snake robots, backbone curves of the form (2) were advocated.[64–67] However, a linear superposition of that form does not obey the internal constraints of the structure. For example, as discussed previously, an inextensible continuum structure incapable of stretching should have $\epsilon(t) = 0$. But such a constraint cannot be enforced with (2).

A way to achieve the same intent of dimensionality reduction in (2) while observing realistic physical constraints of the slender structure is to restrict intrinsic parameters such as curvature and extensibility to have a modal form.[20,68,69] In the planar case,

$$R(\tau)\mathbf{e}_1 = \begin{pmatrix} \cos\theta(\tau) \\ \sin\theta(\tau) \end{pmatrix}$$

where the angle $\theta(\tau)$ is related to the curvature of a plane curve by the simple formula

$$\theta(t) = \int_0^t [1+\epsilon(\tau)]\kappa(\tau)\mathrm{d}\tau.$$

The 'intrinsic' modal approach then amounts to setting

$$\kappa(\tau) = \sum_{k=1}^{m_1} a_k \phi_k(\tau)\,; \quad \epsilon(\tau) = \sum_{k=1}^{m_2} \alpha_k \psi_k(\tau). \tag{3}$$

For example, to position an object in the plane with an inextensible continuum filament, where $\epsilon(\tau) \equiv 0$, we can choose

$$\phi_1(\tau) = 2\pi\cos 2\pi\tau \quad \text{and} \quad \phi_2(\tau) = 2\pi\sin 2\pi\tau$$

resulting in

$$x_{ee} = \cos(a_2) J_0\left[(a_1^2+a_2^2)^{\frac{1}{2}}\right]$$
$$y_{ee} = \sin(a_2) J_0\left[(a_1^2+a_2^2)^{\frac{1}{2}}\right]$$

where J_0 is the zeroth-order Bessel function.

Then the inverse kinematics problem can be solved as

$$a_1 = \pm\left(\left[J_0^{-1}\left[(x_{ee}^2+y_{ee}^2)^{\frac{1}{2}}\right]\right]^2 - [\mathrm{Atan2}(y_{ee}, x_{ee})]^2\right)^{\frac{1}{2}}$$
$$a_2 = \mathrm{Atan2}(y_{ee}, x_{ee})$$

Alternatively, to position an object in the plane while allowing constant stretch, we can have $m_1 = m_2 = 1$ with $\phi_1(\tau) = \tau$ and $\psi_1 = 1$. Then the result will be a circular arc of curvature and length that depends on the two variables a_1 and α_1 that has a simple closed-form parametric expression.[9]

Interestingly, within this framework, it is even possible to choose modes in curvature as Dirac delta functions. Then [68]

$$\epsilon = 0\,; \quad \kappa(s) = \theta_1\delta(s) + \theta_2\delta(s-L_1) + \theta_3\delta(s-L_1-L_2)$$

causes (1) to result in the forward kinematic equations for a three-link revolute planar manipulator. And, on the other hand, as discussed earlier, the curve model based on (1) can be thought of as an infinite serial chain of concatenated (potentially extensible) links each of infinitesimal length.

The generalization of this modal approach to the spatial case requires some additional mathematical machinery. Both this and how to 'fit' a discrete-chain slender structure to a continuous backbone curve are discussed in the next section.

2.2. Fitting

This backbone curve might represent the centerline of a needle or cannula, or it might be an artificial construct to which a highly articulated (hyper-redundant) manipulator is supposed to adhere, to facilitate planning. For a hyper-redundant manipulator that is modular in nature, it can be broken up into segments, and each segment can be identified with a piece of backbone curve, $[t_i, t_{i+1}]$. The 'fitting' of the actual device to the curve requires that information about the orientation of reference frames attached to the curve at t_i and t_{i+1} also be provided. In principle, any smoothly evolving set of reference frames of the form $\{R(t)\,|\,t \in [0,1]\}$ will suffice, where $R(t) = [\mathbf{u}(t), \mathbf{n}_1(t), \mathbf{n}_2(t)]$, $\mathbf{n}_1(t)$ and $\mathbf{n}_2(t)$ are unit vectors satisfying the condition $\mathbf{n}_1(t)\cdot\mathbf{n}_2(t) = 0$, and $\mathbf{u}(t)\times\mathbf{n}_1(t) = \mathbf{n}_2(t)$.

Then, the combination of backbone curve and evolving set of reference frames can be written as a set of pairs

$$g(t) = (R(t), \mathbf{x}(t)) \in SO(3)\times\mathbb{R}^3.$$

Let $g_i = (R(t_i), \mathbf{x}(t_i))$. Such pairs describe rigid body motions and are endowed with a natural composition operation:

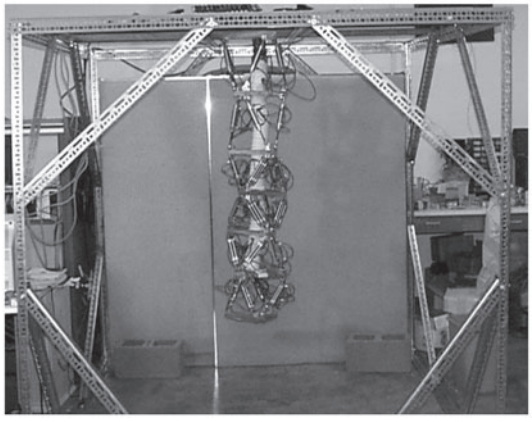

Figure 1. A binary-actuated snakelike robot developed in the author's lab by Dr. Imme Ebert-Uphoff.[70]

$$(R_1, \mathbf{x}_1) \circ (R_2, \mathbf{x}_2) = (R_1 R_2,\, R_1 \mathbf{x}_2 + \mathbf{x}_1) \tag{4}$$

that makes the set of all such pairs a group (the Special Euclidean group), $SE(3)$.

The position and orientation of a reference frame attached at $t = t_{i+1}$ relative to $t = t_i$ is then

$$[g(t_i)]^{-1} \circ g(t_{i+1}) = \Big([R(t_i)]^T R(t_{i+1}),\; [R(t_i)]^T (\mathbf{x}(t_{i+1}) - \mathbf{x}(t_i)) \Big)$$

where $\circ$ denotes the composition of rigid body motions. This relative rigid body motion dictates what the shape of the ith kinematically sufficient module in the chain, such as one of the six-legged platforms in Figure 1, must be.

Sometimes it is convenient to represent this group $SE(3)$ with composition law (4) using 4×4 homogeneous transformation matrices of the form

$$H(R, \mathbf{x}) = \begin{pmatrix} R & \mathbf{x} \\ \mathbf{0}^T & 1 \end{pmatrix}.$$

Then

$$H((R_1, \mathbf{x}_1) \circ (R_2, \mathbf{x}_2)) = H(R_1, \mathbf{x}_1)\, H(R_2, \mathbf{x}_2).$$

Moreover, the body-fixed description of a rigid body velocity can be computed as

$$[H(R(t), \mathbf{x}(t))]^{-1} \frac{\mathrm{d}}{\mathrm{d}t} [H(R(t), \mathbf{x}(t))] = \begin{pmatrix} \Omega & \mathbf{v} \\ \mathbf{0}^T & 0 \end{pmatrix}$$

where $\Omega = R^T \dot{R}$ and $\mathbf{v} = R^T \dot{\mathbf{x}}$. It is often convenient to associate with the 3×3 skew-symmetric matrix Ω the unique vector $\boldsymbol{\omega} \in \mathbb{R}^3$ such that $\Omega \mathbf{x} = \boldsymbol{\omega} \times \mathbf{x}$ where $\times$ is the vector cross product. By a slight abuse of notation (by double usage of $\vee$ and blurring the distinction between $H(g)$ and g), we say that

$$\boldsymbol{\omega} = (R^T \dot{R})^\vee \quad \text{and} \quad \begin{pmatrix} \boldsymbol{\omega} \\ \mathbf{v} \end{pmatrix} = (g^{-1} \dot{g})^\vee. \tag{5}$$

For example, if

$$H(g) = \begin{pmatrix} \cos\theta & -\sin\theta & 0 & 0 \\ \sin\theta & \cos\theta & 0 & 0 \\ 0 & 0 & 0 & z \\ 0 & 0 & 0 & 1 \end{pmatrix}$$

then

$$\begin{pmatrix} \boldsymbol{\omega} \\ \mathbf{v} \end{pmatrix} = \begin{pmatrix} 0 & -\dot{\theta} & 0 & 0 \\ \dot{\theta} & 0 & 0 & 0 \\ 0 & 0 & 0 & \dot{z} \\ 0 & 0 & 0 & 0 \end{pmatrix}^\vee = \begin{pmatrix} 0 \\ 0 \\ \dot{\theta} \\ 0 \\ 0 \\ \dot{z} \end{pmatrix}.$$

One can think of the angular velocity vector $\boldsymbol{\omega}(t)$ in (5) as the analogous quantity as $\kappa(t)$ in the planar case. And a natural extension of (3) from Section 3 to the spatial case would be

$$(g^{-1} \dot{g})^\vee = \sum_{k=1}^{m_1} a_k \boldsymbol{\Phi}_k(t).$$

2.3. *Dynamics*

The continuum filament model can be used for inverse kinematics and planning as described previously, and also for estimating dynamic loads. Modeling the dynamics of mechanical systems is usually done with one of two methods: (1) Lagrange's equations of motion; or (2) Newton–Euler equations of motion. Within both methods, there are two different kinds of dynamics: forward and inverse. In forward dynamics, external forces and moments are supplied and the trajectory of the system is simulated. In inverse dynamics, one seeks to find the external forces and moments responsible for an observed motion.

2.3.1. *Coordinate-dependent vs. coordinate-free dynamics*

In the Lagrangian formulation, the equations of motion for an n-degree-of-freedom mechanical system are of the form

$$\frac{\mathrm{d}}{\mathrm{d}t} \left(\frac{\partial T}{\partial \dot{\boldsymbol{\phi}}} \right) - \frac{\partial T}{\partial \boldsymbol{\phi}} + \frac{\partial V}{\partial \boldsymbol{\phi}} = \boldsymbol{\tau} \tag{6}$$

where T and V are, respectively, the kinetic and potential energies of the system, $\boldsymbol{\phi}$ is an n-dimensional array of generalized coordinates (e.g. joint angles in a robotic manipulator) that fully describe the geometry of the system, and $\boldsymbol{\tau}$ is the applied nonconservative force (e.g. joint torques in the context of a manipulator).

It is well known in the field of Robotics that these dynamical equations are written explicitly as

$$M(\boldsymbol{\phi})\ddot{\boldsymbol{\phi}} + C(\boldsymbol{\phi}, \dot{\boldsymbol{\phi}})\dot{\boldsymbol{\phi}} + \mathbf{G}(\boldsymbol{\phi}) = \boldsymbol{\tau}. \tag{7}$$

For example, if the system of interest is a single rigid body with moment of inertia I, and if ZXZ Euler angles are used

so that $\boldsymbol{\phi} = [\alpha, \beta, \gamma]^T$, then

$$M(\boldsymbol{\phi}) = J^T(\boldsymbol{\phi})\mathcal{I}J(\boldsymbol{\phi})$$

where $J((\boldsymbol{\phi})$ is the Jacobian matrix with $\det J(\boldsymbol{\phi}) = \sin\beta$. This means that $M(\boldsymbol{\phi})$ cannot be inverted when $\beta \in \{0, \pi\}$, which defines the singularities in this parameterization. This is significant because to numerically integrate the above equations of motion in the context of forward dynamics problems, $M(\boldsymbol{\phi})$ is inverted at each timestep.

In the Newton–Euler description of a single body, we write

$$m\ddot{\mathbf{x}}_{cm} = \mathbf{F}; \quad \mathcal{I}\dot{\boldsymbol{\omega}} + \boldsymbol{\omega} \times (\mathcal{I}\boldsymbol{\omega}) = \mathbf{N} \tag{8}$$

where $\mathbf{F}$ is the resultant force acting on the body with mass m and $\mathcal{I}$ and $\mathbf{N}$ are, respectively, the moment of inertia and resultant external moment applied to the body (both as described in a reference frame attached to the center of mass of the body). Note that unlike in the case of (7), this equation is *parameter free*, and these equations can be integrated without inverting $J(\boldsymbol{\phi})$ to solve forward dynamics problems because $J(\boldsymbol{\phi})$ is not present in this formulation, unless someone chooses to introduce it via the relationship

$$\boldsymbol{\omega} = J(\boldsymbol{\phi})\dot{\boldsymbol{\phi}}.$$

And the dynamics of a serial chain such as a robotic manipulator can be divided up into a number of bodies, each obeying a different copy of these equations.

2.3.2. *Inverse continuum dynamics*

Unlike in forward dynamics, where singularities in coordinate-dependent formulations of dynamics can cause difficulties, in inverse dynamics both coordinate-dependent and coordinate-free formulations have essentially equal efficacy when modeling finite dimensional systems. But the question
arises as to how to generate the actuator forces and torques to cause a hyper-redundant manipulator to evolve according to a prescribed sequence of shapes.

Since the shape of such a manipulator is already given by a continuous curve (regardless of whether its physical architecture is a continuum filament or a discrete chain), it makes sense to use this information to approximate the dynamics of the underlying structure. This was done in [9] by introducing one more piece of information: the mass density per unit length of the slender snakelike manipulator, $\rho(s)$. Here, we use s to denote the curve parameter so as not to confuse it with the time parameter which describes dynamics – that is, in the context of the present discussion, $\mathbf{x}(s; t)$ denotes at time t a curve parameterized by s. If $s \in [0, 1]$, then the conservation of mass dictates that

$$\int_0^1 \rho(s)\,\mathrm{d}s = m$$

is constant. Of course, this is assuming that the structure is not actuated by hydraulic fluid or some other means that significantly alters the mass of the manipulator as it changes shape.

Under these conditions, the actuator forces and torques due to the static loading due to gravity and dynamic effects of swinging and/or extending a hyper-redundant manipulator arm can be accounted for using a continuum model. In the case when the manipulator has a continuum architecture, the continuum dynamic model is that of the actual structure. But the approximation of the statics and dynamics of a discrete-chain structure as a continuum filament also has value from the perspective of computational efficiency. This is all explained in [9]. With a structure such as the one shown in Figure 1 in mind, the loading on the i^{th} module or platform in the cascade can be computed from the continuum dynamics by matching the reaction forces and torques

$$\frac{\mathrm{d}}{\mathrm{d}t}\int_{i/n}^1 \rho(s)\frac{\partial \mathbf{x}}{\partial t}\,\mathrm{d}s = \mathbf{F}_i(t) + \int_{i/n}^1 \mathbf{b}(s,t)\,\mathrm{d}s$$

and

$$\frac{\mathrm{d}}{\mathrm{d}t}\int_{i/n}^1 \mathbf{x}(s,t) \times \rho(s)\frac{\partial \mathbf{x}}{\partial t}\,\mathrm{d}s = \mathbf{N}_i(t) + \mathbf{x}(i/n,t) \times \mathbf{F}_i(t) + \int_{i/n}^1 \mathbf{x}(s,t) \times \mathbf{b}(s,t)\,\mathrm{d}s$$

where $\mathbf{b}(s, t)$ is the total external load per unit length due to gravity, external contact, etc. at the point along the backbone defined by s. And $\mathbf{F}_i(t)$ and $\mathbf{N}_i(t)$ are the force and moments computed by the model. These are used to compute the internal actuator torques to generate the desired motion of the actual manipulator.

3. Variational calculus: necessary conditions for optimality of backbone curves

In the case of a discrete-architecture hyper-redundant robot, as the physical robot moves, it is desirable that its joints stay near the middle of their range. Whereas the modal approach is convenient, there are no guarantees for any specific choice of modes that the resulting backbone shapes will comply with limits in joint ranges allowable by the actuators. For this reason, 'optimal' backbone curves that locally vary as little as possible while satisfying global end constraints were investigated.[68,71] Variational methods used to compute optimal curve shapes are one of the topics reviewed in this paper, and these methods draw on the mathematical background presented above. For continuum manipulators, shapes that minimize elastic energy while satisfying certain constraints arise naturally in their modeling as well. Similarly, in modeling DNA as well as in modeling the mechanics of passive macroscopic rods, one seeks the minimal-energy shapes of a DNA filament of given stiffness while satisfying end constraints. This section reviews variational calculus from both coordinate-dependent and coordinate-free perspectives.

3.1. The classical coordinate-dependent case

Let $\boldsymbol{\phi} \in D \subset \mathbb{R}^n$ be a vector of local coordinates describing a region of the configuration space of a system. The classical variational problem is that of extremizing a functional of the form

$$I = \int_{t_1}^{t_2} f(\boldsymbol{\phi}, \dot{\boldsymbol{\phi}}, t)\, \mathrm{d}t \tag{9}$$

subject to constraints of the form

$$\int_{t_1}^{t_2} h_i(\boldsymbol{\phi}, t)\, \mathrm{d}t = H_i. \tag{10}$$

The solution to this problem results from introducing Lagrange multipliers, $\boldsymbol{\lambda} = [\lambda_1, \ldots, \lambda_m]^T \in \mathbb{R}^m$ and defining

$$L(\boldsymbol{\phi}, \dot{\boldsymbol{\phi}}, t) = f(\boldsymbol{\phi}, \dot{\boldsymbol{\phi}}, t) + \sum_{i=1}^{m} \lambda_i h_i(\boldsymbol{\phi}, t) \tag{11}$$

so as to satisfy the *Euler–Lagrange equation* [72–75]

$$\frac{\mathrm{d}}{\mathrm{d}t}\left(\frac{\partial L}{\partial \dot{\boldsymbol{\phi}}}\right) - \frac{\partial L}{\partial \boldsymbol{\phi}} = \mathbf{0} \tag{12}$$

as well as end constraints on $\boldsymbol{\phi}(t_1)$ and $\boldsymbol{\phi}(t_2)$, and the constraints in (10). Numerical shooting methods can be used to refine the values of $\dot{\boldsymbol{\phi}}(t_1)$ and $\boldsymbol{\lambda}$ until a solution is reached.

3.2. The coordinate-free case

Although the coordinate-dependent Euler–Lagrange approach has tremendous value in engineering applications, in some scenarios, the associated singularities cause difficulties. For this reason, less-known coordinate-free approaches also have their place. Coordinate-free variational methods are becoming popular in both the mechanics of quasi-static behavior of elastic rods [76] and in the simulation of rigid body motions.[77] These two problems are very closely related to each other with the main difference being that in the former, the independent variable is arc length and in the latter, it is time. But in both instances, this independent variable traces out a path in space. The distinction between the two problems only becomes significant when the path in space self-intersects. This is unimportant for a rigid body moving in time, but two points on a bent static elastic rod marked by different values of arc length cannot physically occupy the same location in space. In particular, the formulation presented here builds on the formulation in [78].

When the configuration space of a system (such as a rigid body, or reference frames attached to a snakelike robot) has the structure of a Lie group, the problem can be formulated in terms of extremizing functionals of the form

$$I = \int_{t_1}^{t_2} f(g; g^{-1}\dot{g}; t)\, \mathrm{d}t \tag{13}$$

where $g(t)$ is an element of a matrix Lie group G (such as the group of 3×3 rotation matrices, $SO(3)$, or 4×4 homogeneous transformations, $SE(3)$ reviewed earlier in this paper) and $g^{-1}\dot{g}$ is simply the product of the matrices representing g^{-1} and $\dot{g}$, the latter of which is not an element of G.

Given a functional of the form equation (13), and constraint equations of the form

$$\int_{t_1}^{t_2} h_k(g)\, \mathrm{d}t = H_k \tag{14}$$

the necessary conditions for extremizing (13) can then be written in terms of the functions f and h_k as

$$\frac{\mathrm{d}}{\mathrm{d}t}\left(\frac{\partial f}{\partial \xi_i}\right) + \sum_{j,k=1}^{n} \frac{\partial f}{\partial \xi_k} C_{ij}^k \xi_j = \tilde{E}_i^r \left(f + \sum_{l=1}^{m} \lambda_l h_l\right) \tag{15}$$

where $\boldsymbol{\xi} = [\xi_1, \ldots, \xi_n]^T = (g^{-1}\dot{g})^\vee$ contains the independent nonzero entries in the matrix $g^{-1}\dot{g}$ (e.g. angular velocities when $G = SO(3)$, or infinitesimal twists when $G = SE(3)$), $\tilde{E}_i^r$ is a generalization of a directional derivative (defined explicitly below), and $\{C_{ij}^k \mid i, j, k = 1, \ldots, n\}$ is a set of constants called the structure constants, which are fixed for any given G and choice of extracting ξ's from $g^{-1}\dot{g}$. That is, $\xi_i = (g^{-1}\dot{g}, E_i)$ where $\{E_i\}$ is a basis for the Lie algebra of G, and $(\cdot, \cdot)$ is an inner product on this Lie algebra. Explicitly, if the Lie bracket is taken to be the matrix commutator,

$$[A, B] \doteq AB - BA,$$

then C_{ij}^k is defined with respect to the basis $\{E_i\}$ by the equality

$$[E_i, E_j] = \sum_{k=1}^{n} C_{ij}^k E_k.$$

Natural basis elements for $SO(3)$, for which $n = 3$, are

$$E_1 = \begin{pmatrix} 0 & 0 & 0 \\ 0 & 0 & -1 \\ 0 & 1 & 0 \end{pmatrix};$$

$$E_2 = \begin{pmatrix} 0 & 0 & 1 \\ 0 & 0 & 0 \\ -1 & 0 & 0 \end{pmatrix};$$

$$E_3 = \begin{pmatrix} 0 & -1 & 0 \\ 1 & 0 & 0 \\ 0 & 0 & 0 \end{pmatrix}$$

and a natural inner product in this case is $(A, B) \doteq \frac{1}{2}\mathrm{tr}(A^T B)$ resulting in the orthonormality condition $(E_i, E_j) = \delta_{ij}$. The matrices $\{E_i\}$ are well-known in kinematics, and have the property that for any $\mathbf{v} \in \mathbb{R}^3$, $E_i\mathbf{v} = \mathbf{e}_i \times \mathbf{v}$ where $\times$ is the cross product, and $\{\mathbf{e}_i\}$ are the natural unit basis vectors, i.e. $\mathbf{e}_1 = [1, 0, 0]^T$; $\mathbf{e}_2 = [0, 1, 0]^T$; and $\mathbf{e}_3 = [0, 0, 1]^T$. Another connection between the cross product and the geometry of $SO(3)$ is that the structure constants for the corresponding Lie algebra $SO(3)$ are $C_{ij}^k = \epsilon_{ijk}$, the Levi-Civita alternating symbol, which can be used to define the cross product in component form.

In this context,

$$(\tilde{E}_i^r f)(g) \doteq \left.\frac{\mathrm{d}}{\mathrm{d}t} f(g \circ \exp(tE_i))\right|_{t=0} \tag{16}$$

is akin to a directional derivative. For example, if $G = SO(3)$ and $f(R) = r_{11} = \mathbf{e}_1^T R \mathbf{e}_1$ is the first entry of the rotation matrix $R \in SO(3)$, then the derivative $(\tilde{E}_1^r f)(R)$ is computed as

$$\left.\frac{\mathrm{d}}{\mathrm{d}t} \mathbf{e}_1^T R(\mathbb{I} + tE_1)\mathbf{e}_1\right|_{t=0} = \mathbf{e}_1^T R E_1 \mathbf{e}_1 = 0.$$

In the first term above, we can replace $\exp(tE_1)$ with $\mathbb{I} + tE_1$ because ultimately this derivative is only concerned with what happens when t is very small. Since the result contains terms constant and linear in t, only the linear term is retained, and $\mathrm{d}t/\mathrm{d}t = 1$. Finally, the value of zero for this derivative is obtained because $E_1\mathbf{e}_1 = \mathbf{e}_1 \times \mathbf{e}_1 = \mathbf{0}$.

Equation (15) is a modified version of the *Euler–Poincaré* equation, which is a coordinate-free version of the Euler–Lagrange equation in (12). For a derivation and discussion of its history see [79]. Though (15) may seem exotic and difficult to understand for the reader who has not seen it before, there are common instances of it in the equations of mechanics commonly used in Robotics. For example, when $G = \mathbb{R}^n$, then $\xi_i = \dot{\phi}_i$, $C_{ij}{}^k = 0$, and $\tilde{E}_i^r = \partial/\partial\phi_i$ and (15) becomes (6) for the case of no external nonconservative forces. Moreover, if $G = SO(3)$ and $\xi_i = \omega_i$ and $f(\boldsymbol{\omega}) = \frac{1}{2}\boldsymbol{\omega}^T \mathcal{I}\boldsymbol{\omega}$(the kinetic energy of a rigid body), then $C_{ij}{}^k = \epsilon_{ijk}$ (the alternating symbol) and (15) become Euler's equation of motion in (8). For other Lie groups including $SE(3)$, basis elements for the Lie algebras are described in detail in [79–81].

Both the Euler–Lagrange and Euler–Poincaré equations have been used in the modeling of snakelike robots. A point that is often glossed over when these equations are applied is that (12) and (15) provide only *necessary* conditions for optimality. And in general, there is no guarantee that the resulting solution will be optimal in the sense intended by the user. However, in some applications involving snakelike robots, it can be shown that globally optimal solutions result from this formulation.

4. Globally optimal reparameterization of backbone curves

Suppose that an arc length-parameterized curve $\mathbf{x}(s) \in \mathbb{R}^3$ is given, and that the shape of this curve is desirable (e.g. a curve that satisfies end kinematics constraints by the modal approach). If the joint limits of a physical manipulator with discrete architecture are unable to attain a shape consistent with this backbone, but the backbone curve has desirable properties such as built-in obstacle avoidance, then all is not lost. The curve can be 'reparameterized' in a way that effectively slides different sections of the manipulator by different amounts along the backbone curve, expanding some and contracting others. For example, we may start with an arc length-parameterized curve and we may wish to introduce a new curve parameter t such that $s = s(t)$ with the property that the integral of a cost functional of the form

$$f(s, \dot{s}) \doteq \tilde{f}\left(\mathbf{x}(s), \frac{\mathrm{d}\mathbf{x}}{\mathrm{d}s}\dot{s}\right) = \frac{1}{2} m(s)\dot{s}^2$$

is minimized over $0 \le t \le 1$ subject to the constraints that $s(0) = 0$ and $s(1) = 1$, where

$$m(s) \doteq \left(\frac{\mathrm{d}\mathbf{x}}{\mathrm{d}s}\right)^T G(\mathbf{x}(s)) \left(\frac{\mathrm{d}\mathbf{x}}{\mathrm{d}s}\right)$$

and $G(\mathbf{x})$ is a given a weighting matrix. This is the curve reparameterization problem. The intent of such a cost function is to reparameterize in a way that compresses modules in the chain as they go around a tight bend and expands them in straight regions. Referring back to Figure 1, when each platform (or module) is fully extended, it does not have the ability to bend. But if all but a few legs in the platform are short, then the platform has greater ability to bend.

Though in general the Euler–Lagrange equations only provide *necessary* conditions for optimality, this is a special case in which the structure of the function $f(\cdot)$ will guarantee that the solution generated by the Euler–Lagrange equations is a globally optimal solution, as explained in [82].

More generally, suppose that a globally minimal solution to a variational optimization problem with $f_1(\boldsymbol{\phi}, \dot{\boldsymbol{\phi}}, t) = \frac{1}{2}\dot{\boldsymbol{\phi}}^T M(\boldsymbol{\phi})\dot{\boldsymbol{\phi}}$ and $\boldsymbol{\phi}(0)$ and $\boldsymbol{\phi}(1)$ specified has been solved via the Euler–Lagrange equations and minimization over all resulting paths that connect the specified end points. As explained in [82], this solution then can be used to 'bootstrap' a globally optimal solution to a larger variational problem in which the integrand of the functional is

$$f_2(\boldsymbol{\phi}, \boldsymbol{\theta}, \dot{\boldsymbol{\phi}}, \dot{\boldsymbol{\theta}}, t) = \frac{1}{2}\dot{\boldsymbol{\phi}}^T M(\boldsymbol{\phi})\dot{\boldsymbol{\phi}} + \frac{1}{2}\|\dot{\boldsymbol{\theta}} - B(\boldsymbol{\phi})\dot{\boldsymbol{\phi}}\|_W^2 \tag{17}$$

where $\|B\|_W^2 = \mathrm{tr}(B^T W B)$ is the weighted Frobenius norm where $W = W^T > 0$.

Let the solution to the Euler–Lagrange equations for the original variational problem

$$\frac{\mathrm{d}}{\mathrm{d}t}\left(\frac{\partial f_1}{\partial \dot{\boldsymbol{\phi}}}\right) - \frac{\partial f_1}{\partial \boldsymbol{\phi}} = \mathbf{0} \tag{18}$$

be denoted as $\boldsymbol{\phi}^*(t)$.

As explained in [82], when f_2 is of the form in (17), the Euler–Lagrange equations for the new system,

$$\frac{\mathrm{d}}{\mathrm{d}t}\left(\frac{\partial f_2}{\partial \dot{\boldsymbol{\phi}}}\right) - \frac{\partial f_2}{\partial \boldsymbol{\phi}} = \mathbf{0}$$

and

$$\frac{\mathrm{d}}{\mathrm{d}t}\left(\frac{\partial f_2}{\partial \dot{\boldsymbol{\theta}}}\right) - \frac{\partial f_2}{\partial \boldsymbol{\theta}} = \mathbf{0}$$

reduce to (18) and

$$\dot{\boldsymbol{\theta}} - B(\boldsymbol{\phi})\dot{\boldsymbol{\phi}} = \mathbf{a} \tag{19}$$

where $\mathbf{a}$ is a constant vector of integration. Since we postulated the existence of the globally optimal solution $\boldsymbol{\phi}^*(t)$ for (18), all that needs to be done to globally optimize the new problem is to use this in combination with

$$\boldsymbol{\theta}^*(t) = \mathbf{a}t + \mathbf{b} + \int_0^t B(\boldsymbol{\phi}^*(s))\dot{\boldsymbol{\phi}}^*(s)\,\mathrm{d}s \tag{20}$$

where $\mathbf{b}$ is another constant vector that can be matched to boundary values. The global optimality of the solution $(\boldsymbol{\phi}^*(t), \boldsymbol{\theta}^*(t))$ is guaranteed by the assumption that optimal $\boldsymbol{\phi}^*(t)$ is obtained a priori, and the global optimality of $\boldsymbol{\theta}^*(t)$ in (20) can be observed by substituting any $\boldsymbol{\theta}(t) = \boldsymbol{\theta}^*(t) + \boldsymbol{\epsilon}(t)$ where $\boldsymbol{\epsilon}(0) = \boldsymbol{\epsilon}(1) = \mathbf{0}$ into the cost function and observing that

$$\frac{1}{2}\int_0^1 \|\mathbf{a} + \dot{\boldsymbol{\epsilon}}\|_W^2\,\mathrm{d}t = \frac{1}{2}\mathbf{a}^T W\mathbf{a} + \mathbf{a}^T W\int_0^1 \dot{\boldsymbol{\epsilon}}\,\mathrm{d}t + \frac{1}{2}\int_0^1 \|\dot{\boldsymbol{\epsilon}}\|_W^2\,\mathrm{d}t$$

never improves the cost because the second term

$$\int_0^1 \dot{\boldsymbol{\epsilon}}\,\mathrm{d}t = \boldsymbol{\epsilon}(1) - \boldsymbol{\epsilon}(0) = \mathbf{0}$$

vanishes and the third term is nonnegative. That is, adding any nonzero function $\boldsymbol{\epsilon}(t)$ to $\boldsymbol{\theta}^*(t)$ can only increase the cost. This proves that $\boldsymbol{\theta}^*(t)$ is globally optimal.

As a concrete application of this class of problems, consider the problem of simultaneous *curve reparameterization and optimal roll distribution*. Start with an initially arc length-parameterized curve $\mathbf{x}(s)$ for $s \in [0, 1]$, and frames defined using the Frenet–Serret apparatus.[83] If the Frenet frames are $(R_{FS}(s), \mathbf{x}(s))$, then a new set of smoothly evolving reference frames can be defined as $(R(t), \mathbf{x}(t)) = (R_{FS}(s(t))R_1(\theta(s(t))), \mathbf{x}(s(t)))$, where $R_1(\theta)$ is an added twist, or roll, of the Frenet frames about the tangent. Given a cost of the form

$$C \doteq \frac{1}{2}\int_0^1 \left\{\frac{1}{2}r^2\mathrm{tr}(\dot{R}\dot{R}^T) + \dot{\mathbf{x}}\cdot\dot{\mathbf{x}}\right\}\mathrm{d}t = \frac{1}{2}\int_0^1 \left\{(r^2\kappa^2(s) + 1)\dot{s}^2 + r^2(\tau(s)\dot{s} + \dot{\theta})^2\right\}\mathrm{d}t$$

(where r is a specified constant with units of length, and $\kappa(s)$ and $\tau(s)$ are, respectively, the curvature and torsion of the curve), the goal is to find a simultaneous reparameterization $s = s(t)$, and $\theta(s(t))$ so as to minimize C.

The integrand here is of the form in (17) with s taking the place of $\boldsymbol{\phi}$ and θ taking the place of $\boldsymbol{\theta}$. Since the curve reparameterization problem (with the second term in the integral set to zero) is a one-dimensional (1D) variational problem with $f(s, \dot{s}, t) = \frac{1}{2}m(s)(\dot{s})^2$, global optimality is preserved. And from the discussion above, this guarantees the global optimality of the composite problem.

As a result, the sorts of simultaneous curve reparameterization and optimal roll distribution derived in [68,71] from variational calculus in the context of 'hyper-redundant' (snakelike) robotic arms are in fact globally optimal. This is relevant to modeling continuum manipulators constructed of soft rubbery materials because it is not necessarily the case that they are inextensible, and allowing reference frames to redistribute along the backbone curve in a way that is not pegged to arc length may be more realistic in some scenarios. Moreover, for discrete architecture hyper-redundant manipulators, the backbone curve is an artificial construct used to facilitate planning. And forcing a manipulator to adhere to an arc length-parameterized curve to attain an overall shape may not be the best strategy in comparison to allowing it the greater internal freedom afforded by simultaneous minimization of curvature–curve parameter as described in [68,71].

5. Computing optimal curve shapes

The previous section addressed how to redistribute reference frames along a given curve in a globally optimal way. In this section, the synthesis of curves that satisfy the necessary conditions for optimality specified in variational calculus is reviewed both from the coordinate-dependent and coordinate-free perspectives.

5.1. *Coordinate-dependent formulation of optimal curve shape*

Using variational calculus to optimally reparameterize and 're-frame' a space curve as described in the previous section is one of several kinds of variational problems encountered both in hyper-redundant manipulator kinematics and in DNA mechanics. Another variational calculus problem relevant to both fields is that of finding minimal energy shapes of elastic rods subject to end constraints. If $B = B^T \in \mathbb{R}^{3\times 3}$ is the stiffness matrix describing the relative resistance of an inextensible and shearless elastic filament to bending and twisting, then the local cost of deviating from $\boldsymbol{\omega}(s) = \mathbf{b}$ (a constant value describing the unstressed straight or helical shape of the filament) will be $\frac{1}{2}[\boldsymbol{\omega}(s) - \mathbf{b}]^T B[\boldsymbol{\omega}(s) - \mathbf{b}]$. The total potential energy of bending and twisting will be this quantity integrated over the filament. When expressed in coordinates, $\mathbf{q}(s)$, that parameterize the rotation group $SO(3)$ as $R(\mathbf{q})$, then

$$\boldsymbol{\omega}(s) = J(\mathbf{q})\,\dot{\mathbf{q}}$$

where $J(\mathbf{q})$ is the Jacobian matrix relating the rate of change of coordinates to the angular velocity, and the resulting functional will be

$$f(\mathbf{q}, \dot{\mathbf{q}}, s) = \frac{1}{2}[J(\mathbf{q})\,\dot{\mathbf{q}} - \mathbf{b}]^T B[J(\mathbf{q})\,\dot{\mathbf{q}} - \mathbf{b}]$$

(with arc length s taking the place of t in this scenario of an inextensible filament, and $\cdot$ denoting $d/\mathrm{d}s$). This fits within the classical Euler–Lagrange framework. (Here f could depend explicitly on s if $B = B(s)$ were a stiffness that changed along the length of the filament.)

This approach has the problem that all three-parameter descriptions of rotation have singularities where the determinant $\det(J) = 0$. Some parameterizations are worse than others. For example, ZXZ or ZYZ Euler angles will have the singularity corresponding to $R(\alpha, \beta, \gamma)\mathbf{e_3} = \pm\mathbf{e_3}$, which means that if the filament is rooted with an initial direction at its base of $\mathbf{e_3}$, then the Euler–Lagrange equations will be singular. However, other parameterizations such as the exponential coordinates have singularities pushed far away. See [79,80] for discussions of various parameterizations and their relative merits. In the section that follows, the coordinate-free approach is explained.

5.2. Coordinate-free variational equations for backbone curves

Here, the necessary conditions for coordinate-free variational minimization of the energy functionals describing elastic rods subject to end constraints are reviewed. This is a straightforward application of the Euler–Poincaré equations. In the inextensible and shearless case, the group $G = SO(3)$ and in the extensible case, the group is $G = SE(3)$. In both cases, there are six free degrees of freedom to specify the end position and orientation of the elastic filament. In the extensible case, these degrees of freedom correspond to the six scalar components of the initial conditions of $\boldsymbol{\xi}(0)$ where $\boldsymbol{\xi} = (g^{-1}\dot{g})^{\vee}$ which is the body-fixed description of rigid body velocity. In the inextensible case, the six free parameters correspond to three scalar initial conditions $\boldsymbol{\omega}(0)$ where $\boldsymbol{\omega} = (R^T\dot{R})^{\vee}$ is the body-fixed description of angular velocity, and three scalar Lagrange multipliers (components of $\boldsymbol{\lambda}$) corresponding to the three constraints that define $\mathbf{x}(L)$ in the constraint equation (21) given below. For more detailed treatments of the results presented in this section see [78,79,84].

5.2.1. Cost function for minimally bending and twisting backbone curves

For arc length-parameterized backbone curves

$$\mathbf{x}(L) = \int_0^L \mathbf{u}(s)\,\mathrm{d}s \quad \text{and} \quad \mathbf{u}(s) = R(s)\mathbf{e}_3. \tag{21}$$

This can be viewed as the inextensible filament 'growing' along the direction indicated by the tangent for each value of arc length, s, up to a total length of L.

In this case, the stiffness matrix, B, is 3×3, and the resulting problem becomes one of minimizing

$$I = \frac{1}{2}\int_0^L [\boldsymbol{\omega}(s) - \mathbf{b}]^T B[\boldsymbol{\omega}(s) - \mathbf{b}]\mathrm{d}s \tag{22}$$

subject to the constraints (21). Here $\boldsymbol{\omega} = (R^T\,\mathrm{d}R/\mathrm{d}s)^{\vee}$ and $\mathbf{b}$ are angular velocities as seen in the body-fixed frame, where arc length s replaces time as the independent variable.

Unlike the extensible problem, which was an unconstrained variational minimization problem on $SE(3)$, this is a constrained variational problem on $SO(3)$, and will therefore involve the use of Lagrange multipliers. The Euler–Poincaré equations for both cases are worked out below.

5.2.2. The Euler–Poincaré equations for inextensible rods

Considering the case of (22) with the kinematic constraint of inextensibility (21), one writes Eq. (15) with $f = U$ for $i = 1, 2, 3$ together as the vector equation

$$B\dot{\boldsymbol{\omega}} + \boldsymbol{\omega} \times (B\boldsymbol{\omega} - \mathbf{b}) = \begin{pmatrix} -\boldsymbol{\lambda}^T R\mathbf{e}_2 \\ \boldsymbol{\lambda}^T R\mathbf{e}_1 \\ 0 \end{pmatrix} \tag{23}$$

where a dot represents differentiation with respect to arc-length s and $\boldsymbol{\lambda} \in \mathbb{R}^3$ is the vector of Lagrange multipliers necessary to enforce the vector constraint in Eq. (21).

For example, if B is diagonal with entries B_1, B_2, B_3, then the above can be written in component form as

$$\begin{aligned} &B_1\dot{\omega}_1 + \omega_2(B_3\omega_3 - b_3) - \omega_3(B_2\omega_2 - b_2) \\ &\quad = -\lambda_1 R_{12} - \lambda_2 R_{22} - \lambda_3 R_{32}; \\ &B_2\dot{\omega}_2 + \omega_3(B_1\omega_1 - b_1) - \omega_1(B_3\omega_3 - b_3) \\ &\quad = \lambda_1 R_{11} + \lambda_2 R_{21} + \lambda_3 R_{31}; \\ &B_3\dot{\omega}_3 + \omega_1(B_2\omega_2 - b_2) - \omega_2(B_1\omega_1 - b_1) = 0. \end{aligned}$$

But more generally, the matrix B could have off-diagonal coupling terms.

Eq. (23) is solved iteratively, subject to the initial conditions $\boldsymbol{\omega}(0) = \boldsymbol{\mu}$ which are varied together with the Lagrange multipliers until $\mathbf{x}(L)$ and $R(L)$ attain the desired values. $R(s)$ is computed from $\boldsymbol{\omega}(s)$ in Eq. (23) by integrating the matrix differential equation

$$\dot{R} = R\left(\sum_{i=1}^{3} \omega_i(s)E_i\right),$$

and $\mathbf{x}(L)$ is then obtained from Eq. (21). Numerical methods for updating $\boldsymbol{\mu}$ and $\boldsymbol{\lambda}$ so as to push the position and orientation of the distal end to specified values are described in [78], in which minimal energy conformations of DNA with different amounts of end twist were computed, resulting in the shapes in Figure 2.

This figure shows single energy-minimizing conformation for each end condition. This assumes that the DNA stiffness is known accurately, and there is some debate in the literature as to what the exact stiffness parameters are. DNA is a relatively stiff molecule and is often modeled as a homogeneous elastic rod. For fairly long DNA fragments (longer than about 100 nm), this wormlike chain model provides a description that correlates well with experiments such as force spectroscopy.[85–87] Another way to determine stiffness parameters is to let DNA molecules float down to a flat surface and then using atomic force microscopy (AFM) to scan the resulting 2D shapes.[88] The ensemble of such shapes can then be used to extract the $SE(2)$ diffusion matrix to fit the appropriate continuum model, as explained

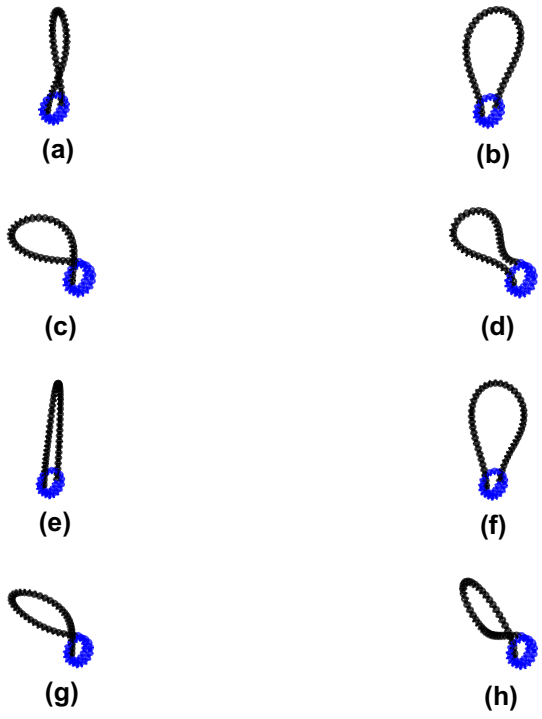

Figure 2. DNA conformations as solutions to variational calculus problem.[78] Subfigures (a)-(h) show loop shapes for elastic filaments with different stiffness and chirality as originally derived in the PhD dissertation of Dr. Jin Seob Kim.

in [89,90]. Such information can be fused with that obtained from other experimental modalities, such as 3D pulling experiments or light scattering to obtain the best estimate of DNA stiffness.

5.3. Concentric tube robots

Concentric tube robots (or active canulae) consist of n concentric elastic tubes that have been pre-bent. Several research groups have investigated these sorts of snakelike robots, including [12,13] and work referenced therein. One analysis method that is applicable to these robots is a variational approach, as presented in [91]. Indeed, the use of the Euler–Poincaré equations in this application follows in much the same way as for the derivation of optimal backbone curves for hyper-redundant manipulators. The tubes are essentially inextensible, and so the energy due to deformation can be written as

$$E = \frac{1}{2}\sum_{i=1}^{n}\int_0^1 [\boldsymbol{\omega}_i'(s)]^T B_i(s)[\boldsymbol{\omega}_i'(s)]\,\mathrm{d}s \qquad (24)$$

where $\boldsymbol{\omega}_i'(s) = \boldsymbol{\omega}_i(s) - \boldsymbol{\omega}_i^*(s)$ and $\boldsymbol{\omega}_i^*(s)$ describes the equilibrium shape of the i^{th} tube which has 3×3 stiffness matrix $B_i(s)$. All tubes have the same length and initial and final positions and orientations. As a result, determining the equilibrium shape is a matter of determining $\boldsymbol{\omega}_1(s)$ and the relative angles (and angular rates) that the other tubes exhibit relative to this. As explained in [91],

$$\boldsymbol{\omega}_i(s) = \exp(-\theta_i(s)E_3)\,\boldsymbol{\omega}_1(s) + \dot{\theta}_i(s)\,\mathbf{e}_3$$

where $\mathbf{e}_3 = [0,0,1]^T$ and E_3 is the skew-symmetric matrix such that $E_3\mathbf{x} = \mathbf{e}_3 \times \mathbf{x}$ and $\theta_i(s)$ is the amount of twist that each tube $i = 2,3,\ldots,n$ undergoes relative to tube 1, consistent with the boundary conditions imposed. Since the 1D rotations described by each of the θ_i are in $SO(2)$, the Euler–Poincaré formulation can be (and has been) employed successfully with

$$G = SO(3) \times SO(2) \times \cdots \times SO(2)$$

to determine the equilibrium conformations.

5.4. Kinematic needle-steering models

Two kinds of variational problems arise in steering of flexible needles in soft tissues. First, when the tissue is firm and does not deform substantially as the needle is inserted, the optimal control problem of how to push and twist the needle 'as little as possible' while still reaching the goal presents itself. Second, if the tissue is soft, the question of how the potential energy in the needle and that in the tissue equilibrate becomes a significant problem. Both of these issues are variational in nature, and efforts that have already been published are reviewed, and future directions are sketched here.

When a flexible needle with a sharp beveled tip is inserted into firm tissue, it has a tendency to follow a roughly circular path. This results in a 3D version of a 'unicycle' model described in [6]. This model was extended to the 'bicycle' model in [8]. In the unicycle model, the reference frame attached to the needle tip executes a trajectory of the form

$$\begin{pmatrix} \dot{R} & \dot{\mathbf{x}} \\ \mathbf{0}^T & 0 \end{pmatrix} = \begin{pmatrix} R & \mathbf{x} \\ \mathbf{0}^T & 1 \end{pmatrix}\begin{pmatrix} \Omega & \mathbf{v} \\ \mathbf{0}^T & 0 \end{pmatrix}$$

where

$$\begin{pmatrix} \Omega & \mathbf{v} \\ \mathbf{0}^T & 0 \end{pmatrix} = \begin{pmatrix} 0 & -\omega(t) & 0 & 0 \\ \omega(t) & 0 & -\kappa & 0 \\ 0 & \kappa & 0 & v(t) \\ 0 & 0 & 0 & 0 \end{pmatrix}$$

where κ is the constant curvature of the path that a needle naturally wants to follow, and $(\omega(t), v(t)$ are the control inputs. See, for example, [92] for notation and [93] for an up-to-date survey on the field of flexible needle steering. The variational problem then becomes that of minimizing the control cost

$$C_1 = \frac{1}{2}\int_0^1 \left\{c_1(\omega(t))^2 + c_2(v(t))^2\right\}\mathrm{d}t$$

subject to the boundary conditions $g(0) = (\mathbb{I}, \mathbf{0})$ and $g(1) = g_d$ (the desired target frame). A practical problem that is encountered is the lack of repeatability of observed needle-steering trajectories. Building on the prior work in [94], this has been modeled as a stochastic version of the above kinematic constraint in [6], and probabilistic methods on Lie groups have been employed to solve the problem.[92,95]

For other aspects of continuum robot modeling see [96–104].

6. Conclusions

Highly articulated and flexible manipulators were reviewed. Variational methods are shown to be a useful tool for modeling and planning motions of these structures. For hyper-redundant manipulators, which have many articulated degrees of freedom, variational methods are useful in defining slowly varying backbone curves, as well as an optimal distribution of reference frames that evolve along it. For concentric tube (active cannula) robots, variational methods provide the solution to the equilibrium conformations resulting from the interaction of the tubes, and in needle-steering problems, the variational approach provides a tool for planning trajectories. It is shown that these same methods are applicable to modeling DNA conformations subjected to end constraints.

Disclosure statement

No potential conflict of interest was reported by the author.

Funding

The author was supported by the NSF under an IPA contract while serving as a program director. The ideas expressed are the author's and do not necessarily express those of the NSF.

Notes on contributor

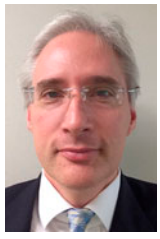

G.S. Chirikjian received undergraduate degrees from Johns Hopkins University in 1988, and the PhD degree from the California Institute of Technology, Pasadena, in 1992. Since 1992, he has been on the faculty of the Department of Mechanical Engineering, Johns Hopkins University, where he has been a full professor since 2001. From 2004–2007 he served as department chair. His research interests include robotics, applications of group theory in a variety of engineering disciplines, and the mechanics of biological macromolecules. He is a 1993 National Science Foundation Young Investigator, a 1994 Presidential Faculty Fellow, and a 1996 recipient of the ASME Pi Tau Sigma Gold Medal. In 2008, he became a fellow of the ASME, and in 2010, he became a fellow of the IEEE. He is the author of more than 200 journal and conference papers and the primary author for three books: Engineering Applications of Noncommutative Harmonic Analysis (2001) and Stochastic Models, Information Theory, and Lie Groups, Vols. 1+2. (2009, 2011).

References

[1] Hirose S. Biologically inspired robots: serpentile locomotors and manipulators. Oxford: Oxford University Press; 1993.
[2] Ma S. Analysis of creeping locomotion of a snake-like robot. Adv. Robot. 2001;15:205–224.
[3] Wolf A, Brown HB, Casciola R, et al. A mobile hyper redundant mechanism for search and rescue tasks. In: Proceedings 2003 IEEE/RSJ International Conference on Intelligent Robots and Systems (IROS 2003); October 27–31; Vol. 3; Las Vegas, NV; 2003. p. 2889–2895.
[4] Simaan N, Taylor R, Flint P. A dexterous system for laryngeal surgery. In: Proceedings 2004 IEEE International Conference on Robotics and Automation, ICRA '04; 2004 April 26–May 1; Vol. 1; New Orleans, LA: 2004. p. 351–357.
[5] Murphy RJ, Kutzer MDM, Chirikjian GS, et al. Constrained workspace generation for snake-like manipulators with applications to minimally invasive surgery. In: Proceedings of the 2013 IEEE International Conference on Robotics and Automation (ICRA 2013); May; Karlsruhe 2013. p. 5341–5347.
[6] Park W, Kim JS, Zhou Y, et al. 2005. Diffusion-based motion planning for a nonholonomic flexible needle model. In: Proceedings of the IEEE International Conference on Robotics and Automation; April; Barcelona, Spain. 6 p.
[7] Alterovitz R, Lim A, Goldberg K, et al. 2005. Steering flexible needles under Markov motion uncertainty. In: Proceedings of the IEEE/RSJ International Conference on Intelligent Robots and Systems; Edmonton; August. p. 120–125.
[8] Webster RJ III, Kim J-S, Cowan NJ, et al. Nonholonomic modeling of needle steering. Int. J. Robot. Res. 2006;25:509–525.
[9] Chirikjian GS. Hyper-redundant manipulator dynamics: a continuum approximation. Adv. Robot. 1995;9:217–243.
[10] Neppalli S, Csencsits MA, Jones BA, et al. Closed-form inverse kinematics for continuum manipulators. Adv. Robot. 2009;23:2077–2091.
[11] Sears P, Dupont P. A steerable needle technology using curved concentric tubes. In: 2006 IEEE/RSJ International Conference on Intelligent Robots and Systems; October 9–15; Beijing; 2006. p. 2850–2856.
[12] Dupont PE, Lock J, Itkowitz B, et al. Design and control of concentric-tube robots. IEEE Trans. Robot. 2010;26:209–225.
[13] Webster RJ III, Romano JM, Cowan NJ. Mechanics of precurved-tube continuum robots. IEEE Trans. Robot. 2009;25:67–78.
[14] Jones BA, Walker ID. Kinematics for multisection continuum robots. IEEE Trans. Robot. 2006;22:43–55.
[15] Mochiyama H. 2005. Hyper-flexible robotic manipulators. In: 2005 IEEE International Symposium on Micro-NanoMechatronics and Human Science; Nagoya; November. p. 41–46.
[16] Xiao J, Vatcha R. Real-time adaptive motion planning for a continuum manipulator. In: 2010 IEEE/RSJ International Conference on Intelligent Robots and Systems (IROS'10); October; Taipei; 2010 p. 5919–5926.
[17] Li J, Teng Z, Xiao J, et al. Autonomous continuum grasping. In: 2013 IEEE/RSJ International Conference on Intelligent Robots and Systems (IROS'13); November; Tokyo; 2013. p. 4569–4576.
[18] Li J, Xiao J. Progressive generation of force-closure grasps for an *n*-section continuum manipulator. In: 2013 IEEE International Conference on Robotics and Automation (ICRA'13); May; Karlsruhe; 2013. p. 4016–4022.
[19] Robinson G, Davies JBC. Continuum robots – a state of the art. IEEE Conf. Robot. Autom. Detroit, MI; 1999;2849–2854.
[20] Chirikjian GS, Burdick JW. An obstacle avoidance algorithm for hyper-redundant manipulators. In: Proceedings of the IEEE Robotics and Automation Conference; May 13–18; Cincinnati, OH; 1990. p. 625–631.

[21] Renda F, Giorelli M, Calisti M, et al. Dynamic model of a multibending soft robot arm driven by cables. IEEE Trans. Robot. 2014;30;1–14.
[22] Yekutieli Y, Sagiv-Zohar R, Aharonov R, et al. Dynamic model of the octopus arm. I. Biomechanics of the octopus reaching movement. J. Neurophys. 2005;94:1443–1458.
[23] Boyer F, Ali S, Porez M. Macrocontinuous dynamics for hyper-redundant robots: application to kinematic locomotion bioinspired by elongated body animals. IEEE Trans. Robot. 2012;28:303–317.
[24] Boxerbaum AS, Shaw KM, Chiel HJ, et al. Continuous wave peristaltic motion in a robot. Int. J. Robot. Res. 2012;31:302–318.
[25] Camarillo DB, Milne CF, Carlson CR, et al. Mechanics modeling of tendon-driven continuum manipulators. IEEE Trans. Robot. 2008;24:1262–1273.
[26] Kim B, Ha J, Park FC, et al. Optimizing curvature sensor placement for fast, accurate shape sensing of continuum robots. In: Proceedings of IEEE International Conference on Robotics and Automation (ICRA'14); May; Hong Kong; 2014. p. 5374–5379.
[27] Chen Y, Liang J, Hunter IW. Continuum robotic endoscope design and path planning. In: Proceedings of IEEE International Conference on Robotics and Automation; May; Hong Kong; 2014. p. 5593–5540.
[28] Jeon J, Yi B-J. Shape prediction algorithm for flexible endoscope. In: Proceedings of IEEE International Conference on Robotics and Automation; May; Hong Kong; 2014. p. 2856–2861.
[29] Steigmann DJ, Faulkner MG. variational theory for spatial rods. Arch. Rational Mech. Anal. 1993;133:1–26.
[30] Simo JC, Vu-Quoc L. A three dimensional finite-strain rod model. Part II: computational aspects. Comput. Meth. Appl. Mech. Eng. 1986;58:79–116.
[31] Love AEH. A treatise on the mathematical theory of elasticity. New York (NY): Dover; 1944.
[32] Daniels HE. The statistical theory of stiff chains. Proc. Roy. Soc. (Edinburgh). 1952;A63:290–311.
[33] Hermans JJ, Ullman R. The statistics of stiff chains, with applications to light scattering. Physica. 1952;18:951–971.
[34] Kratky O, Porod G. Röntgenuntersuchung Gelöster Fadenmoleküle. Recueil des Travaux Chimiques des Pays-Bas. 1949;68:1106–1122.
[35] Gobush W, Yamakawa H, Stockmayer WH, et al. Statistical mechanics of wormlike chains. I. Asymptotic behavior. J. Chem. Phys. 1972;57:2839–2843.
[36] Kamein RD, Lubensky TC, Nelson P, et al. Direct determination of DNA twist-stretch coupling. Europhys. Lett. 1997;28:237–242.
[37] Moroz JD, Nelson P. Torsional directed walks, entropic elasticity, and DNA twist stiffness. Proc. Nat. Acad. Sci. USA. 1997;94:14418–14422.
[38] Marko JF, Siggia ED. Bending and twisting elasticity of DNA. Macromolecules. 1994;27:981–988.
[39] Levene SD, Crothers DM. Ring closure probabilities for DNA fragments by Monte Carlo simulation. J. Mol. Biol. 1986;189:61–72.
[40] Nelson P. Sequence-disorder effects on DNA entropic elasticity. Phys. Rev. Lett. 1998;80:5810.
[41] Odijk T. Stiff chains and filaments under tension. Macromolecules. 1995;28:7016–7018.
[42] Purohit PK, Kondev J, Phillips R. Mechanics of DNA packaging in viruses. Proc. Nat. Acad. Sci. 2003;100:3173–3178.
[43] Spakowitz AJ, Wang Z-G. End-to-end distance vector distribution with fixed end orientations for the wormlike chain model. Phys. Rev. E. 2005;72:041802.
[44] Tu ZC, Ou-Yang ZC. Elastic theory of low-dimensional continua and its applications in bio-and nano-structures. J. Comput. Theor. Nanosci. 2008;5:422–448.
[45] Vologodskii A. Topology and physics of circular DNA. Boca Raton: CRC Press; 1992.
[46] Wolgemuth CW, Sun SX. Elasticity of α-helical coiled coils. Phys. Rev. Lett. 2006;97:248101.
[47] Nelson PC. Spare the (elastic) rod. Science. 2012;337:1045–1046.
[48] Vafabakhsh R, Ha T. Extreme bendability of DNA less than 100 base pairs long revealed by single-molecule cyclization. Science. 2012;337:1097–1101.
[49] Benham CJ. Elastic model of the large-scale structure of duplex DNA. Biopolymers. 1979;18:609–23.
[50] Benham CJ, Mielke SP. DNA mechanics. Annual Rev. Biomed. Eng. 2005;7:21–53.
[51] Coleman BD, Tobias I, Swigon D. Theory of the influence of end conditions on self-contact in DNA loops. J. Chem. Phys. 1995;103:9101–9109.
[52] Coleman BD, Swigon D, Tobias I. Elastic stability of DNA configurations. II: supercoiled plasmides with self-contact. Phys. Rev. E. 2000;61:759–770.
[53] Balaeff A, Mahadevan L, Schulten K. Modeling DNA loops using the theory of elasticity. E-print archive arXiv.org; 2003. Available from: http://arxiv.org/abs/physics/0301006.
[54] Balaeff A, Mahadevan L, Schulten K. Structural basis for cooperative DNA binding by CAP and Lac repressor. Structure. 2004;12:123–132.
[55] Coleman BD, Olson WK, Swigon D. Theory of sequence-dependent DNA elasticity. J. Chem. Phys. 2003;118:7127–7140.
[56] Coleman BD, Dill EH, Lembo M, et al. On the dynamics of rods in the theory of Kirchhoff and Clebsch. Arch. Rational Mech. Anal. 1993;121:339–359.
[57] Gonzalez O, Maddocks JH. Extracting parameters for base-pair level models of DNA from molecular dynamics simulations. Theor. Chem. Acc. 2001;106:76–82.
[58] Goyal S, Perkins NC, Lee CL. Nonlinear dynamics and loop formation in Kirchhoff rods with implications to the mechanics of DNA and cables. J. Comp. Phys. 2005;209:371–389.
[59] Chirikjian GS, Burdick JW. Kinematics of hyper-redundant robot locomotion. IEEE Trans. Robot. Autom. 1995;11:781–793.
[60] Burdick JW, Radford J, Chirikjian GS. A sidewinding locomotion gait for hyper-redundant robots. Adv. Robot. 1995;9:195–216.
[61] Vaidyanathan R, Chiel HJ, Quinn RD. A hydrostatic robot for marine applications. Robot. Auton. Syst. 2000;30:103–113.
[62] Transeth AA, Pettersen KY, Liljebäck P. A survey on snake robot modeling and locomotion. Robotica. 2009;27:999–1015.
[63] Pettersen KY, Stavdahl O, Gravdahl JT. Snake robots: modelling, mechatronics, and control. New York, NY: Springer; 2013.
[64] Hayashi A, Park J, Kuipers BJ. 1990. Toward planning and control of highly redundant manipulators. In: Proceedings of the 5th IEEE International Symposium on Intelligent Control; Philadelphia, PA; 1990 September; IEEE. p. 683–688.

[65] Naccarato F, Hughes P. Inverse kinematics of variable-geometry truss manipulators. J. Robot. Syst. 1991;8:249–266.
[66] Salerno RJ, Reinholtz CF, Dhande SG. Kinematics of long-chain variable geometry truss manipulators. Amsterdam: Springer; 1991.
[67] Zanganeh KE, Angeles J. The inverse kinematics of hyper-redundant manipulators using splines. In: Proceedings of the 1995 IEEE International Conference on Robotics and Automation; May; Vol. 3; Nagoya; 1995. p. 2797–2802.
[68] Chirikjian GS. Theory and applications of hyper-redundant robotic manipulators. Division of engineering and applied science, California Institute of Technology; Pasadena, CA; 1992.
[69] Chirikjian GS, Burdick JW. A modal approach to hyper-redundant manipulator kinematics. IEEE Trans. Robot. Autom. 1994;10:343–354.
[70] Ebert-Uphoff I. On the development of discretely-actuated hybrid-serial-parallel manipulators [PhD dissertation]. Department of Mechanical Engineering, Johns Hopkins University; 1997.
[71] Chirikjian GS, Burdick JW. Kinematically optimal hyper-redundant manipulator configurations. IEEE Trans. Robot. Autom. 1995;11:794–806.
[72] Brechtken-Manderscheid U. Introduction to the calculus of variations. New York (NY): Chapman and Hall; 1991.
[73] Ewing GM. Calculus of variations with applications. New York: W.W. Norton and Co.; 1969.
[74] Gruver WA, Sachs E. Algorithmic methods in optimal control. Boston: Pitman Publishing Ltd; 1980.
[75] Kamien MI, Schwartz NL. Dynamic optimization: the calculus of variations and optimal control in economics and management. New York (NY): North-Holland; 1991.
[76] Bretl T, McCarthy Z. Quasi-static manipulation of a Kirchhoff elastic rod based on a geometric analysis of equilibrium configurations. Int. J. Robot. Res. 2014;33: 48–68.
[77] Lee T, Leok M, McClamroch NH. Lie group variational integrators for the full body problem. Comput. Meth. Appl. Mech. Eng. 2007;196:2907–2924.
[78] Kim J-S, Chirikjian GS. Conformational analysis of stiff chiral polymers with end constraints. Mol. Simul. 2006;32:1139—1154.
[79] Chirikjian GS. Stochastic models, information theory, and Lie groups. Vols. 1+2. Boston: Birkhäuser; 2009/2012.
[80] Chirikjian GS, Kyatkin AB. Harmonic analysis for engineers and applied scientists. Dover; 2015.
[81] Chirikjian GS, Kyatkin AB. An operational calculus for the Euclidean motion group with applications in robotics and polymer science. J. Fourier Anal. Appl. 2000;6:583–606.
[82] Chirikjian GS. Variational analysis of Snakelike robots. In: Milutinović D, Rosen J, editors. Redundancy in robot manipulators and multi-robot systems. Vol. 57, Lecture notes in electrical engineering. Springer; 2013. p. 77–91.
[83] Chirikjian GS. Framed curves and knotted DNA. Biochem. Soc. Trans. 2013;41:635–638.
[84] Chirikjian GS. Group theory and biomolecular conformation, I.: mathematical and computational models. J. Phys.: Condens. Matter. 2010;22:323103.
[85] Bustamante C, Marko JF, Siggia ED, et al. Entropic elasticity of lambda-phage DNA. Science. 1994;265:1599–1600.
[86] Bustamante C, Smith SB, Liphardt J, et al. Single-molecule studies of DNA mechanics. Curr. Opinion Struct. Biol. 2000;10:279–285.
[87] Nelson P. Biological physics: energy, information, life. New York (NY): WH Freeman; 2004.
[88] Rivetti C, Guthold M, Bustamante C. Scanning force microscopy of DNA deposited onto mica: equilibration versus kinetic trapping studied by statistical polymer chain analysis. J. Mol. Biol. 1996;264:919–932.
[89] Wolfe KC, Chirikjian GS. Signal detection on Euclidean groups: applications to DNA bends, robot localization, and optical communication. IEEE J. Selected Topics Signal Process. 2013;7:708–719.
[90] Wolfe KC, Hastings WA, Dutta S, et al. Multiscale modeling of double-helical DNA and RNA: a unification through Lie groups. J. Phys. Chem. B. 2012;116:8556–8572.
[91] Rucker C, Webster RJ III, Chirikjian GS, et al. Equilibrium conformations of concentric-tube continuum robots. Int. J. Robot. Res. 2010;29:1263–1280.
[92] Park W, Wang Y, Chirikjian GS. The path-of-probability algorithm for steering and feedback control of flexible needles. Int. J. Robot. Res. 2010;29:813–830.
[93] Cowan NJ, Goldberg K, Chirikjian GS, et al. Robotic needle steering: design, modeling, planning, and image guidance. In: Rosen J, Hannaford B, Satava R, editors. Surgical robotics – systems, applications, and visions. Springer; 2011. p. 557–582.
[94] Zhou Y, Chirikjian GS. Probabilistic models of dead-reckoning error in nonholonomic mobile robots. In: ICRA'03; September; Taipei, Taiwan; 2003.
[95] Wang Y, Chirikjian GS. Nonparametric second-order theory of error propagation on the Euclidean group. Int. J. Robot. Res. 2008;27:1258–1273.
[96] Chirikjian GS, Burdick JW. Parallel formulation of the inverse kinematics of modular hyper-redundant manipulators. In: Proceedings of the IEEE Robotics and Automation Conference; April; 1991. p. 708–713.
[97] Choset H, Lynch KM, Hutchinson S, et al. Principles of robot motion: theory, algorithms, and implementations. MIT Press; 2005.
[98] Galloway KC, Polygerinos P, Walsh CJ, et al. 2013. Mechanically programmable bend radius for fiber-reinforced soft actuators. In: 2013 International Conference on in Advanced Robotics (ICAR'13); November. p. 1–6.
[99] Lobaton EJ, Fu J, Torres LG, et al. Continuous shape estimation of continuum robots using X-ray images. IEEE Int. Conf. Robot. Autom. 2013;725–732.
[100] Rone WS, Ben-Tzvi P. Continuum robot dynamics utilizing the principle of virtual power. IEEE Trans. Robot. 2014;30:275–287.
[101] Suzumori K, Iikura S, Tanaka H. Development of flexible microactuator and its applications to robotic mechanisms. In: ICRA 1991; April; 1991. p. 1622–1627.
[102] Trivedi D, Rahn CD, Kier WM, et al. Soft robotics: Biological inspiration, state of the art, and future research. Appl. Bionics Biomech. 2008;5:99–117.
[103] Wang YF, Chirikjian GS. Workspace generation of hyper-redundant manipulators as a diffusion process on SE(N). IEEE Trans. Robot. Autom. 2004;20:399–408.
[104] Wolfe KC, Mashner M, Chirikjian GS. Bayesian fusion on Lie groups. J. Algebraic Stat. 2011;2:75–97.